NASA TECHNICAL NOTE

NASA TN D-2986

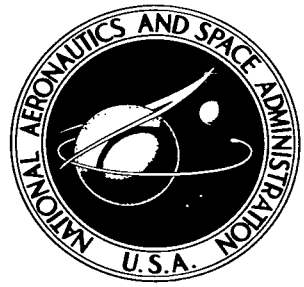

NASA TN D-2986

INFLUENCE OF OPPOSING SLITS ON MOLECULAR FLOW FROM AN ISOTHERMAL ENCLOSURE AT LOW DENSITIES

by Eugene J. Manista and John W. Sheldon

Lewis Research Center
Cleveland, Ohio

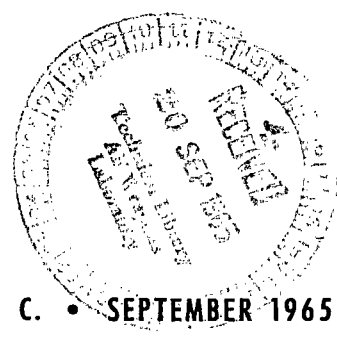

NATIONAL AERONAUTICS AND SPACE ADMINISTRATION • WASHINGTON, D. C. • SEPTEMBER 1965

INFLUENCE OF OPPOSING SLITS ON MOLECULAR FLOW FROM AN ISOTHERMAL ENCLOSURE AT LOW DENSITIES

By Eugene J. Manista and John W. Sheldon

Lewis Research Center
Cleveland, Ohio

NATIONAL AERONAUTICS AND SPACE ADMINISTRATION

For sale by the Clearinghouse for Federal Scientific and Technical Information
Springfield, Virginia 22151 – Price $1.00

INFLUENCE OF OPPOSING SLITS ON MOLECULAR FLOW FROM AN ISOTHERMAL ENCLOSURE AT LOW DENSITIES

by Eugene J. Manista and John W. Sheldon

Lewis Research Center

SUMMARY

A direct particle density measurement of cesium vapor in an isothermal enclosure is described. A surface ionization detector is used to determine the particle flux issuing through a narrow slit in the enclosure. The effect of a second slit located in the rear wall of the enclosure and directly opposite the emitting slit is investigated quantitatively, and the results are analyzed in terms of a hypothetical "hole emission" from the second slit. The attenuation of the "hole" beam is used to determine a cesium-cesium cross section. The result is compared with a previously published cross section obtained by more conventional techniques.

INTRODUCTION

The kinetic-theory equations that govern free-molecule flow from an isothermal enclosure through a thin orifice, or slit, are well established both theoretically and experimentally (Ramsey, ref. 1). In comparing the results of experiment with theory, a question of great significance is how well the actual experimental enclosure approaches the ideal, narrow-slit isothermal enclosure postulated by the theoretical model, wherein the mean free path of the effusing atom is assumed to be greater than both the slit width and slit depth.

In any scattering experiment designed to determine the absolute value of a collision cross section, it is necessary to know the spatial variation of the number density of scattering particles throughout the scattering region. The investigation of atomic interactions at thermal energies usually requires that the scattering particles be in the gas phase. Confinement of the scattering particles is then accomplished by either physically collimating them into an atomic beam or by confining them in a scattering chamber provided with entrance and exit slits in order to allow for the passage of the bombarding

particles. In the crossed-beam technique, the spatial variation in the scattering particle density can be only approximately calculated using the kinetic theory. Hence the method does not lend itself readily to the determination of the absolute value of the collision cross section since the density in the scattering region is not known with sufficient accuracy. By confining the scattering particles to a physical scattering chamber that approaches the ideal, isothermal enclosure the spatial variation in the scattering particle density can be predicted with more certainty along with the energy distribution of the scattering particles.

In studying the cesium-cesium (Cs-Cs) interaction at thermal energies by the beam transmission method, some interesting effects have been noticed associated with the efflux of Cs scattering atoms from a scattering chamber at low scattering-particle densities. The purpose of this note is to describe the effects and to point out some of the problems involved in making an accurate density determination of the scattering vapor in the chamber. A simple kinetic theory analysis of the efflux of atoms at low densities from an isothermal enclosure is also presented and compared with experimental results. The number-density determination of Cs is compared with the number densities calculated from previous vapor pressure data (ref. 2). Aside from the actual number density data the simple theory also yields a method for estimating the total cross section for the Cs-Cs interaction at thermal energies.

FORMULATION OF THE "HOLE" EFFECT

The partial flow of particles from an ideal isothermal enclosure is given by the well-known equation (Ramsey, ref. 1)

$$\Gamma = \frac{n\bar{v}}{4\pi} \cos\theta \, A_s \, d\Omega \tag{1}$$

(Symbols are defined in appendix A.) In this equation, Γ is the number of particles per second passing into the solid angle $d\Omega$ that lies at a polar angle of θ relative to the direction of the outward normal from the source area A_s. The particles inside the enclosure have a uniform density of n atoms per cubic centimeter and a Maxwellian velocity distribution in thermal equilibrium with the walls characterized by the mean velocity $\bar{v}$, in centimeters per second.

Figure 1 is a schematic of the apparatus used in the present investigations. A horizontal view of the collimation system is shown in more detail in figure 2. The flux of cesium atoms from the exit slit of the scattering chamber Γ is directly measured in terms of the ion current to the Langmuir-Taylor detector since cesium atoms incident on a hot

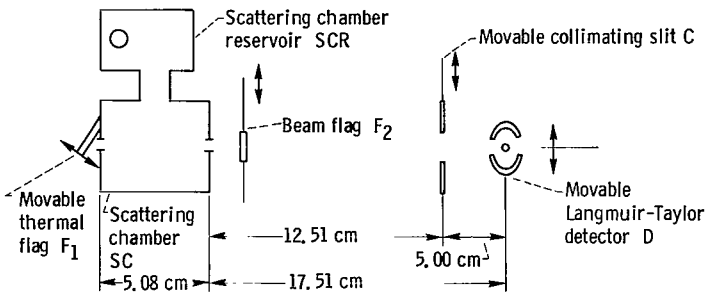

Figure 1. - Schematic of experimental layout.

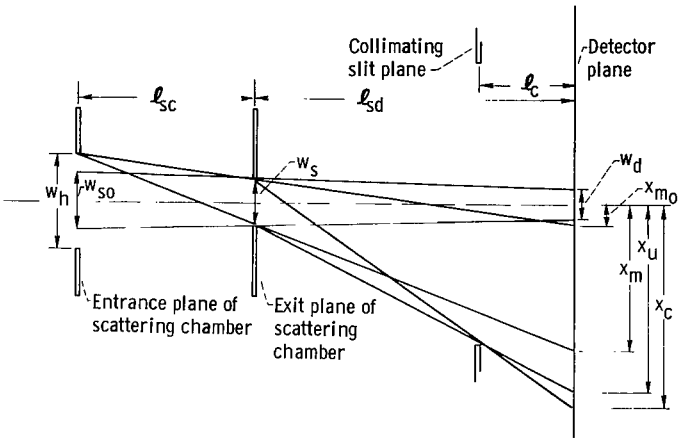

Figure 2. - Top view of collimation system (not to scale).

tungsten filament are converted to ions with close to 100-percent efficiency (Datz and Taylor, ref. 3). The particle current is given by

$$I = \frac{ne\bar{v}}{4\pi} A_s \frac{A_d}{\ell^2} \qquad (2)$$

In equation (2), I is the measured current in amperes, e is the charge on the electron. The solid angle $d\Omega$ has been replaced by the ratio of the detector area A_d to the square of the distance from the source to the detector ℓ, and $\cos\theta$ has been set equal to one since the maximum lateral displacement of the detector is small compared to the distance ℓ.

Equation (2) describes the current from an ideal enclosure over the entire free molecular flow regime. The only additional condition for the validity of equation (2) is that the loss of particles through the slit does not affect the phase-space distribution of particles inside.

Consider, however, the effect of placing an additional slit on the wall, directly opposite the exit slit. The slit area is made nearly as small as the exit slit, so that the flux out both slits still has little influence on the distribution inside. The question then arises as to whether or not the additional slit influences the flux distribution out the exit slit. The answer can be seen clearly by going to the limit of low densities in the enclosure; that is, by letting the mean free path of the particle exceed the characteristic dimension of the enclosure. Under this condition, collisions with the wall greatly exceed any volume collisions, and hence the only way a particle can exit the enclosure within a specified solid angle is for it to originate at the opposite wall. Therefore, if a direct line of sight through both slits is established, the particle flux along that line will be diminished accordingly as to whether a uniform wall is seen or whether the slit through the opposite wall is seen.

In order to be able to formulate the above considerations, the assumption is made that the slit in the isothermal wall emits "holes" that are the absence of the real particles that would be emitted from the chamber wall if the slit in the wall did not exist; that

is, they contribute a negative flux from the slit area. Referring to figure 1, the particle flux out the exit slit is then made up of two groups, real particles from a perfect enclosure and holes. (A more detailed discussion and derivation of the equations used in this section are given in appendix B.)

Hence, expressed in terms of a current, the total flux at the detector is

$$I = I_a + I_h \tag{3}$$

where the current due to atoms is given by

$$I_a = \frac{ne\bar{v}}{4\pi} A_s \frac{A_{d_a}}{\ell_{sd}^2} \tag{4a}$$

and, the current due to holes is

$$I_h = I_{ho} e^{-\ell_{sc}/\lambda} \tag{4b}$$

where I_{ho} is the source current of "holes"

$$I_{ho} = -\frac{ne\bar{v}}{4\pi} A_h \frac{A_{d_o}}{(\ell_{sd} + \ell_{sc})^2} \tag{5}$$

A_s is the source area for real particles, A_h is the effective source area for "holes," A_{d_a} and A_{d_o} are the effective beam areas at the detector planes for atoms and "holes," and ℓ_{sd} and $(\ell_{sd} + \ell_{sc})$ are the respective distances from the two sources. Furthermore, it is assumed that "holes" are scattered (eq. (4b)) in exactly the same way as a beam of real particles that enters the scattering chamber; that is, I_{ho} is the source of the "hole" current at the slit and I_h is the "hole" current out the exit slit. In the above λ is the mean free path of the "hole" beam in the scattering chamber and ℓ_{sc} is the length of the scattering chamber.

Combining equations (3), (4), and (5), the following expression can be obtained for the ratio of the particle flux down the line of sight to the maximum flux from an ideal enclosure:

$$\frac{I}{I_a} = 1 - \left(\frac{\ell_{sd}}{\ell_{sd} + \ell_{sc}}\right)\left(\frac{h_{d_o}}{h_{d_a}}\right) e^{-n\ell_{sc}Q} \tag{6}$$

This equation is valid as long as the slits satisfy the mean-free-path requirement. Equation (6) is applicable in the preceding form in those cases where the exit slit width w_s is smaller than the "hole" slit width w_h. In the equation, h_{d_a} is the effective height of the atom beam at the detector plane and h_{d_o} is the effective height of the "hole" beam at the detector plane (see appendix B). The mean free path λ of equation (4b) has been replaced by the effective cross section Q along with the actual particle density of n scatterers per cubic centimeter. In most experimental geometries, the effective height h_{d_o} is nearly equal to the effective height h_{d_a}. The considerations of other geometries is straightforward.

Equation (6) describes the expected behavior of the line of sight particle flux from the enclosure as a function of the density of scattering particles present. The ratio I/I_a has the following limiting values:

$$\lim_{n \to 0} \frac{I}{I_a} = 1 - \left(\frac{\ell_{sd}}{\ell_{sd} + \ell_{sc}} \right) \left(\frac{h_{d_o}}{h_{d_a}} \right) \tag{7}$$

$$\lim_{n \to \infty} \frac{I}{I_a} = 1 \tag{8}$$

Furthermore, a semilogarithmetic plot of $1 - I/I_a$ against the scattering particle density should yield a straight line of negative slope equal to $\ell_{sc}Q$ and an intercept given by $\left[\ell_{sd}/(\ell_{sd} + \ell_{sc})\right] \left(h_{d_o} / h_{d_a} \right)$. Thus from the slope of the straight line the effective cross section Q is determined. The hard sphere averaged total cross section for the Cs-Cs interaction can be calculated as in Rosin and Rabi (ref. 4) from the effective cross section, Q.

The presence of the collimating slit C (fig. 1) can easily be taken into account to yield the expected flux distribution at the detector plane. For $w_s < w_h$, and $w_s < w_c$, straightforward geometric ray calculations yield the following pertinent widths (see fig. 2):

Minimum width of the "hole" beam at detector plane:

$$2x_{m_o} = \frac{\ell_{sd}}{\ell_{sc}} (w_h - w_s) - w_s \qquad \text{or zero, whichever is greater.} \tag{9a}$$

Maximum width of the "hole" beam at the detector plane:

$$2x_m = \frac{\ell_{sd}}{\ell_{sc}} (w_h + w_s) + w_s \tag{9b}$$

Width of the umbra at detector plane:

$$2x_u = w_c + (w_c - w_s) \frac{\ell_c}{\ell_{sd} - \ell_c} \tag{9c}$$

Total cutoff width due to external collimating slit of width w_c:

$$2x_c = \frac{\ell_{sd}}{\ell_{sd} - \ell_c} (w_c + w_s) - w_s \tag{9d}$$

APPARATUS AND PROCEDURE

The vacuum envelope and pumping station along with the more general details of the atomic-beam apparatus employed in this study have been described in an earlier report (Manista and Sheldon, ref. 5). Figure 1 (p. 3) shows the essential details of the experimental arrangement used in the present investigation. The scattering chamber SC and the scattering-chamber reservoir SCR are made of high-conductivity, oxygen-free copper. Both the scattering chamber and the scattering chamber reservoir are mounted on a Supramica (thermal conductivity $\simeq 10^{-3}$ cal/(cm)(sec)(^{o}C)) base in an attempt to eliminate thermal-conduction losses through the base supports. They are connected by a thin-walled stainless-steel transfer tube of 0.50 inch diameter. The scattering chamber and the scattering chamber reservoir are equipped with separately controlled ac heaters that enable the temperatures of each to be independently variable. An extensive iron-constantan thermocouple system monitered and controlled the temperatures of each during the experimental runs. A room-temperature compensated potentiometer measured the thermal emf generated.

The slits are formed from sheets of 0.051-millimeter-thick stainless-steel shim stock in which narrow slits of about 5 millimeters height are cut by an electron-beam technique. Entrance and exit slits are mounted onto the front and rear of the scattering chamber. In normal operation, a beam of cesium atoms produced by an auxiliary oven would enter and leave the scattering chamber through these slits. This beam, however, was not used in the present investigations since the experiments were aimed particularly at determining the effect the entrance slit has on the efflux of cesium-scattering atoms

through the exit slit of the scattering chamber. In order to simulate an isothermal enclosure as a reference in the experiments, a movable thermal flag, F_1 of copper was placed over the entrance slit of the scattering chamber. The flag was constructed such that it was always held in good thermal contact with the scattering chamber and was isolated from the surroundings. The flag could easily be opened or closed from the exterior of the vacuum chamber during the experimental runs.

The flux of cesium atoms that issues from the exit slit of the scattering chamber passes through the movable collimating slit C shown in figure 1 and is ultimately detected by a movable Langmuir-Taylor surface-ionization detector D. The detector is identical to that used in the work reported in reference 5 except that provisions for moving the detector perpendicularly across the beam by means of an external micrometer drive have been incorporated. The relative reproducibility of the detector movement amounted to ±5 microns. The detected particle current was measured by a Cary model 31 electrometer with a response time of 0.1 second. The output of the electrometer was recorded on a strip-chart recorder. An additional beam flag F_2 was located between the scattering chamber and the detector to enable background readings to be observed. A typical ac noise current of 5×10^{-14} ampere was observed at the filament temperature used ($\approx1850^{\circ}$ K). This level is equivalent to a particle flux of about 3×10^{5} atoms per second incident on the detector.

Since it was also of interest to compare the present experimental results with previous determinations of the cesium vapor pressure, extreme care was taken in accurately alining the slits with the detector filament. The initial alinement was done using an optical telescope. The final adjustments were performed using the beam issuing from the scattering chamber as an indicator of the best alinement. In order to be able to reduce the measured particle current to an equivalent density in the scattering chamber, the geometry must be known accurately. The slits and detector filament were measured by comparing their widths against a calibrated reticle under a magnification of 300 in a microscope. The widths are believed accurate to ±1 micron. Table I presents the pertinent

TABLE I. - TYPICAL BEAM PARAMETERS

Entrance slit width, w_h, cm	0.0103
Entrance slit height, h_h, cm	0.500
Exit slit, width, w_s, cm	0.0041
Exit slit width, w_s, cm	0.500
Collimator slit width, w_c, cm	0.102
Collimator slit height, h_c, cm	0.635
Detector diameter, d, cm	0.0055
Detector entrance height, h_d, cm	0.635
Length of SC, ℓ_{sc}, cm	5.08
Distance from exit slit of SC to detector plane, ℓ_{sd}, cm	17.51
Distance from exit slit of SC to collimator plane, $\ell_{sd} - \ell_c$, cm	12.51

geometric details of the experimental arrangement.

About 0.25 gram of high-purity cesium (99.95 percent) contained in a vacuum-loaded Pyrex ampoule was used as the source material for the scattering vapor. The Pyrex ampoule was placed in the well reservoir of the scattering chamber reservoir and could be ruptured by a plunger from the exterior of the chamber. After a thorough pumpdown and bakeout of the scattering chamber and scattering chamber reservoir (300° C for at least 24 hr), the temperatures of the scattering chamber and the scattering chamber reservoir were lowered and held at 110° C. Liquid nitrogen was then added to the cold traps, and the entire apparatus was allowed to come into thermal equilibrium overnight. The background pressure as measured by an ion gage was below 1×10^{-7} torr throughout the experimental runs.

The temperature of the scattering chamber reservoir was lowered to about 80° C and the ampoule containing the cesium was broken. This high reservoir temperature allowed the cesium to coat the interior walls of both the scattering chamber and the scattering chamber reservoir relatively quickly. After equilibrium had occurred (5 to 15 min), the detector was tuned for maximum signal by adjusting both the collimator C and the detector D.

The particle flux distribution with the thermal flag F_1 open and closed was measured by moving the detector D across the beam. Beam profiles were taken at various constant scattering chamber reservoir temperatures in the range of 30° to 90° C. At one point, the collimating slit was purposely shifted off alinement (no direct line of sight through the entrance and exit slits of the scattering chamber) in order to scan only the flux issuing from the exit slit and originating essentially from an interior wall of the scattering chamber. The background level was constantly checked by shuttering the flag F_2.

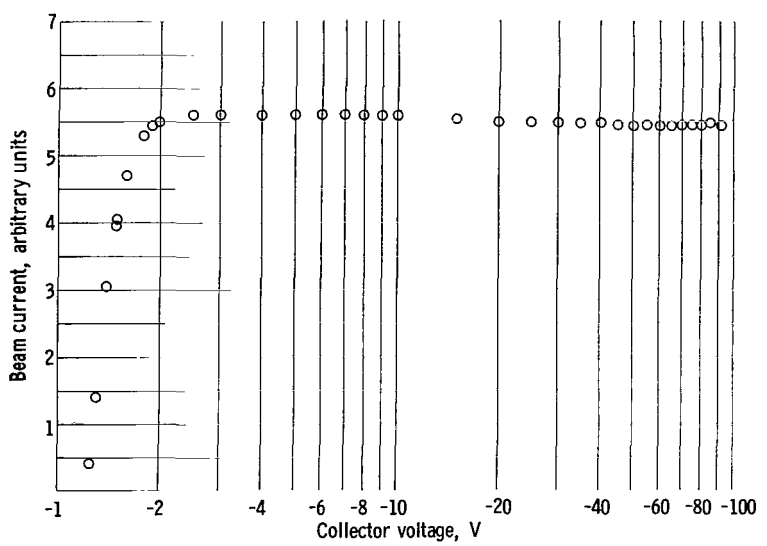

Figure 3. - Ion saturation characteristic of atom detector.

RESULTS AND DISCUSSION

The result of varying the collection voltage of the detector is shown in figure 3. A constant flux of cesium atoms was incident on the detector throughout the time required to obtain the data. The detector filament temperature used was sufficient to ensure nearly 100-percent surface ionization of every atom incident on the hot tungsten surface.

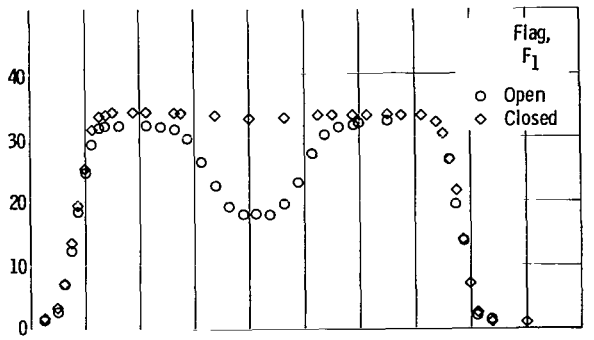

(a) Scattering chamber reservoir temperature approximately 55° C, cesium density approximately 6×10^{11} atoms per cubic centimeter.

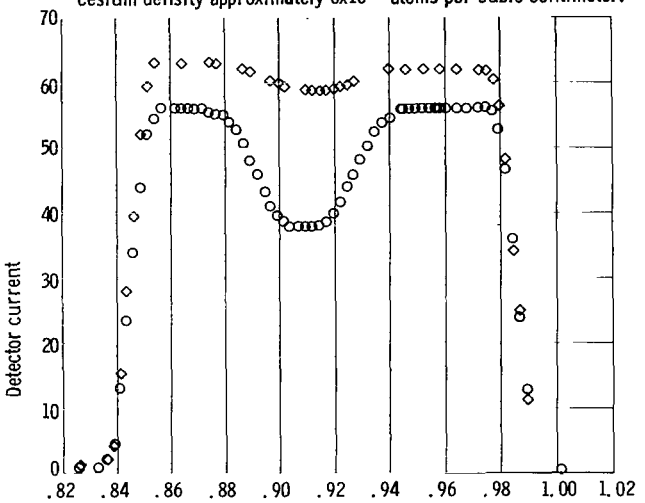

(b) Scattering chamber reservoir temperature 62° C, cesium density approximately 11×10^{11} atoms per cubic centimeter.

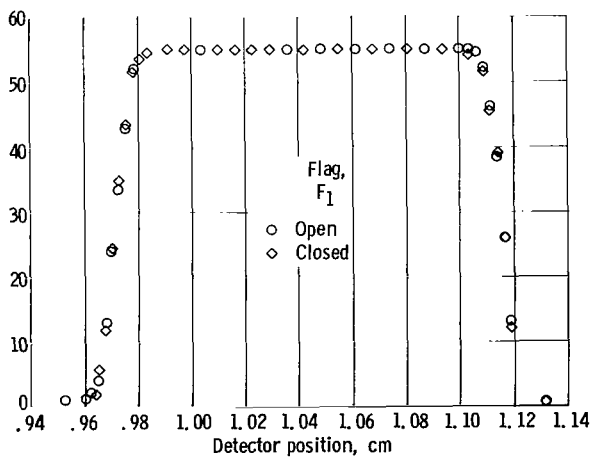

(c) Scattering chamber reservoir temperature 61° C, cesium density approximately 9.8×10^{11} atoms per cubic centimeter. Collimator shifted off line so detector cannot "see" entrance slit.

Figure 4. - Observed cesium flux from scattering chamber at a constant scattering chamber temperature of 110° C.

Normal collection voltage was about -94 volts although the data in figure 3 show that saturation of the ion current can take place at voltages as low as -2.5 volts. The slight decrease in the collected current as the collection voltage was increased could have been due to the loss of accelerated ions through the collector aperture.

Figure 4 shows typical flux distributions observed from the scattering chamber under thermal equilibrium conditions. The data in figure 4(a) correspond to a lower density of cesium in the scattering chamber as compared to the data in figure 4(b). One point immediately apparent from the data is that opening the thermal flag F_1, does indeed cause a reduction in the direct-line-of-sight flux out the exit slit of the scattering chamber. This is evidenced by the dip occurring in the flux distributions. Closing the flag F_1; that is, attempting to simulate an ideal, isothermal enclosure, causes the dip in the flux distribution to become smaller. The residual dip in the central portion of the flux distribution in figure 4(b) with the flag F_1 closed is undoubtedly due to a leakage of the cesium around the periphery of the flag. This view is further substantiated by the flag closed data of figure 4(a) in which the dip is barely noticeable. Other flux distributions taken show that in some cases the flag F_1 sealed the entrance slit tight, while in others it did not seal properly and thus caused a small dip to still appear in the direct line of sight flux.

The time required to reach the equi-

TABLE II. - COMPARISON OF CALCULATED AND

OBSERVED BEAM PROFILES

Dimension	Calculated	Observed
Minimum width of "hole" beam, $2x_{m_o}$, cm	0.017	0.014
Maximum width of "hole" beam, $2x_m$, cm	0.054	0.060
Width of umbra, $2x_u$, cm	0.141	0.125
Total cut-off width, $2x_c$, cm	0.158	0.157

librium level characteristic of the flag F_1 being open or closed was not studied on a rigid quantitative basis. However, some qualitative observations were made. The response of the detector to opening the flag was very rapid, less than a second was necessary to reach the equilibrium value. In closing the flag, however, a time constant of several minutes was observed. At low densities in the scattering chamber, corresponding to scattering chamber reservoir temperatures of about 50° C, a much longer time was necessary than that required when the density was higher (e. g., for scattering chamber reservoir temperatures near 90° C). The time required to reach equilibrium is more than likely associated with the time required to build up a few atomic layers of cesium on the flag after it had essentially rid itself of any previous cesium layers.

The widths of the flux distribution in figures 4(a) and (b) are compared with the widths calculated from equation (9) in table II. The agreement is quite good. Both the minimum width of the "hole" beam $2x_{m_o}$, corresponding to a direct view through both slits, and the maximum width of the "hole" beam $2x_m$, agree with the calculated values within a few percent.

The difference in the magnitude of the detector current at the flat sections on either side of the central dip, for flag closed and open, is due to slightly different reservoir temperatures between the two. These flat regions on either side of the dip are the regions of constant flux that are observed when the detector cannot see directly through both slits, that is, the observed flux is characteristic of a true, isothermal enclosure. The true density of cesium in the scattering chamber is therefore indicated by the current observed in these regions, rather than by the current observed at the central region.

In figure 4(c), the external collimating slit C was shifted from the previous alinement used to observe the direct line of sight flux to a new position from which it was geometrically impossible to see through both slits. The flux distribution from the scattering chamber was observed with F_1 open and closed. The data taken show no evidence of a dip or general decrease in either case. It is concluded from these data that the phase-

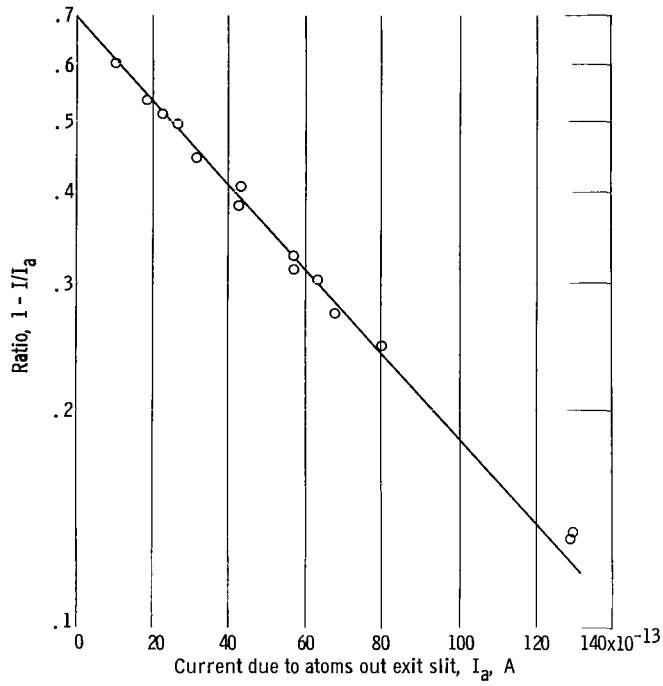

Figure 5. - Attenuation of "hole" beam. The ordinate is the "hole" beam observed at the cesium density corresponding to the observed current of cesium atoms from the scattering chamber.

space distribution describing the particles in the scattering chamber is not significantly influenced by the presence of small slits in the walls of the enclosure and the resulting loss of particles through these slits.

The data shown in figure 5 illustrate the attenuation of the "hole" beam. The current observed in the flat region I_a is proportional to the true particle density in the scattering chamber. Equation (6) predicts a linear dependence of $\ln(1 - I/I_a)$ on particle density. Such a dependence is certainly observed in figure 5. Equation (6) also predicts an intercept of 0.775 if $h_{d_o}/h_{d_a} = 1$. The observed intercept is 0.700 indicating $h_{d_o}/h_{d_a} = 0.928$. A slight vertical misalinement of the relative positions of the slits could account for this difference.

A value of the hard sphere cross section for the "Cs-hole-Cs atom" interaction is obtainable from equation (6) and the attenuation data shown in figure 5. The method of Rosin and Rabi (ref. 4) was used to reduce the measured effective cross section to the actual value of the hard sphere cross section. Equation (4a) was employed to obtain the scattering-atom density in the scattering chamber from the experimentally determined scattering chamber current, I_a. The total cross section found for a mean particle energy corresponding to 383° K was 1430×10^{-16} square centimeter.

This cross section corresponds to the scattering of "holes" through an average angle greater than 4.3 minutes of arc (as calculated from the beam geometry presented in fig. 1, p. 3 and the Kusch criterion; ref. 6). The hypothetical process of "hole scattering" is actually the scattering of cesium atoms emitted from the area surrounding the hole slit through the same angle, 4.3 minutes, into the "hole beam." That is, the scattering of cesium atoms into the "hole beam" makes the "hole beam" appear attenuated. Hence the cross section for Cs-hole-Cs-atom scattering is just the Cs-Cs scattering cross section.

Estermann, Foner, and Stern (ref. 7) have reported a Cs-Cs cross-section value of 2350×10^{-16} square centimeter for a beam temperature of 450° K and an angular resolution of 5 seconds. The difference between the value reported in reference 7 and the value

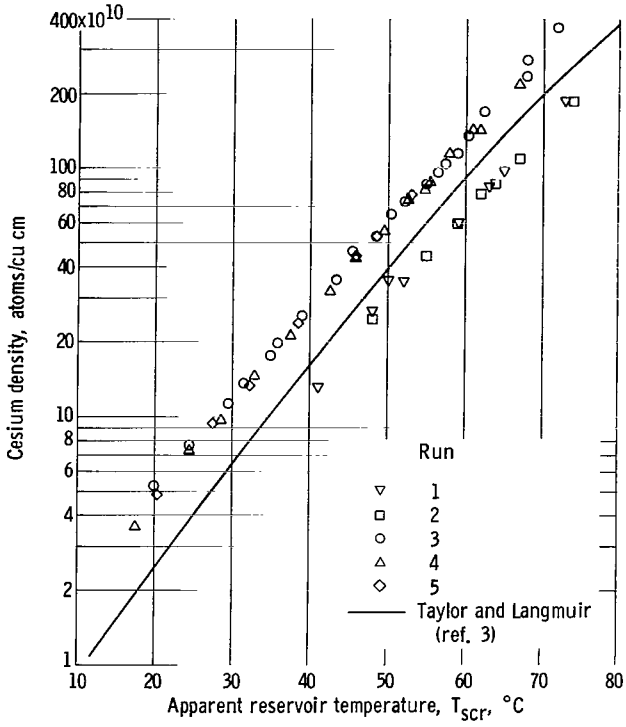

Figure 6. - Comparison of crude vapor pressure (density) determination with Langmuir-Taylor data (ref. 3).

obtained herein can be attributed to the increased angular resolution of reference 7. The total error in the value of the absolute magnitude of the cross section determined herein (for the 4.3 min resolution) is conservatively estimated at ±10 percent. Most of this error is due to the experimental problems involved in determining the proper density of scattering atoms participating in the collisions.

The results found for the cesium vapor density are plotted against the measured reservoir temperature T_{scr} in figure 6. Five sets of datum points are shown. The data of runs 1 and 2 were obtained with a different slit and detector width than those of runs 3 to 5. This was done to eliminate any possible systematic error due to geometry. The results are seen to fall on two self-consistent curves. As can be seen from inspection of the two curves, the internal consistency of the data comprising the two curves is reproducible. The solid curve shown in figure 6 is the vapor density of cesium as determined by Taylor and Langmuir (ref. 2). The Taylor and Langmuir data were corrected for thermal transpiration between the reservoir and the scattering chamber for comparison with the present results. The present results lie on both sides of the Taylor and Langmuir determination, and indicate that a systematic error in measurement accounts for the difference between the runs labeled 1 and 2 and those labeled 3 to 5. Since extreme care was taken in measuring the geometrical factors in equation (4a) (these were known to about 10 percent) in both cases, the most likely reason for the larger differences present in figure 6 is the measured reservoir temperature T_{scr}. This temperature was measured with the same iron-constantan thermocouple in both cases, but the location of the thermocouple was purposely shifted in the two experiments in order to see if any appreciable thermal gradients existed in the reservoir block. In both sets of data, the thermocouple was not in direct physical contact with the cesium pool, but was located near the reservoir pool.

The data shown in figure 6 illustrate that a temperature difference existed between the two thermocouple locations even though the reservoir pool was located in a massive copper block. Since an absolute determination of the cesium vapor pressure was not of primary interest (i. e., knowing the absolute abscissa of fig. 6 very accurately) no ex-

treme precautions were taken to ensure the absence of small thermal gradients in the reservoir block. The data, however, do point out the extreme care that must be taken if an absolute determination is to be attempted. Furthermore, the data illustrate the error that can arise if it is arbitrarily assumed that the lowest temperature measured corresponds to the temperature at the surface of the dominant cesium pool, and the Taylor and Langmuir data are then used to compute the corresponding vapor density, evaporation rate, etc.

CONCLUDING REMARKS

The results of the present investigation were as follows:

1. A "hole" emission hypothesis can be used to explain the observed reduction in the direct line of sight flux issuing from in-line slits of a two-slit isothermal enclosure. The same "hole" hypothesis can be used to obtain an atom-atom cross section consistent with values obtained by more conventional and refined techniques.

2. A direct particle density (or pressure) measurement of an alkali vapor in an isothermal enclosure can be made by observing the particle flux issuing from a thin slit in the wall of the enclosure. However, care must be exercised in alining the detector so that it can only "see" an inside wall representative of the entire enclosure.

3. The assumption that a thermocouple near the "dominant" evaporating pool of alkali measures the true surface temperature of the liquid may be a poor one. The temperature distribution present in the reservoir under operating conditions should be investigated experimentally in order to be reasonably sure of the actual pool temperature.

Lewis Research Center,
National Aeronautics and Space Administration,
Cleveland, Ohio, June 10, 1965.

APPENDIX A

SYMBOLS

A_d	detector area, sq cm
A_{d_a}	effective beam area for atoms at detector plane
A_{d_o}	effective beam area for "holes" at detector plane
A_h	effective source area for "holes"
A_s	source area, sq cm
C	collimating slit
D	Langmuir-Taylor detector
d	half-width of penumbra
$d\Omega$	solid angle
e	electronic charge
F_1	thermal flag
F_2	beam flag
h	height of exit and entrance slits
h_a	height of atom source slit
h_c	height of collimator slit
h_{d_a}	effective height of atom beam at detector plane
h_{d_o}	effective height of "hole" beam at detector plane
h_h	height of "holes" source slit
I	measured current, A
I_a	current due to atoms out exit slit
I_h	current due to "holes" out exit slit
I_{h_o}	source current of "holes"
ℓ	distance from source to detector, cm
ℓ_c	distance from collimator plane to detector plane
ℓ_{sc}	length of scattering chamber
ℓ_{sd}	distance from exit slit of scattering chamber to detector plane
n	number density, particles per cu cm
p	half-width of umbra
p+d	width of equivalent rectangular beam
Q	effective cross section
SC	scattering chamber
SCR	scattering chamber reservoir
T_{sc}	temperature of scattering chamber
T_{scr}	temperature of scattering chamber reservoir
$\bar{v}$	mean velocity, cm/sec
w_c	width of collimator slit
w_d	width of detector
w_h	width of entrance slit

w_s	width of exit slit
w_{so}	effective source width for "holes"
$2x_c$	total cutoff width due to collimating slit at detector plane
$2x_m$	maximum width of "hole" beam at detector plane
$2x_{m_o}$	minimum width of "hole" beam at detector plane
$2x_u$	width of umbra at detector plane
Γ	particle flux, no./sec
θ	polar angle, rad
λ	mean free path

APPENDIX B

BEAM GEOMETRY

The derivation of equation (6) proceeds from equation (2) in the following way: First, note that the collimating system used can, in general, influence both the detected width and height of either the real particle beam or the "hole" beam at the detector plane. In the case considered here, the width of the collimating slit C (fig. 1, p. 3), is larger than the width of the beam of real particles or "holes." Furthermore, the widths of the two beams at the detector plane are large compared to the actual detector width. Hence, the effective detected width is just the actual detector width w_d. In the vertical direction, however, the effective heights of the two beams differ at the detector plane.

In figure 7, h_{d_o} is the effective beam height for "holes," and h_{d_a} is the effective beam height for atoms. In order to evaluate the effective beam heights for the two beams, the height of the equivalent rectangular beam corresponding to each of the two beams is used. Figure 8 shows the expected intensity of particles at the detector plane in the vertical direction for a typical source slit and collimating slit. (See Ramsey, ref. 1 for a complete discussion of beam profiles.) The equivalent rectangular beam height, defined as the height that gives the same total vertical current as the actual beam, is (p + d), where p and d are the half-widths of the umbra and penumbra and can be obtained from equations II-17 to II-19 of reference 1 in terms of slit heights and distances.

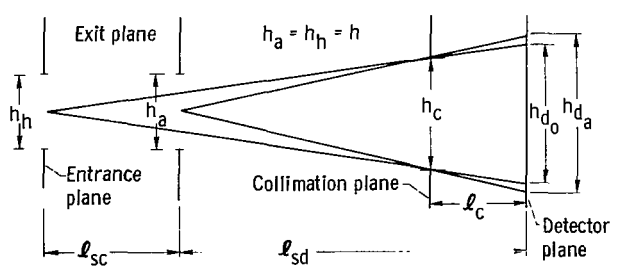

Figure 7. - Vertical collimation system.

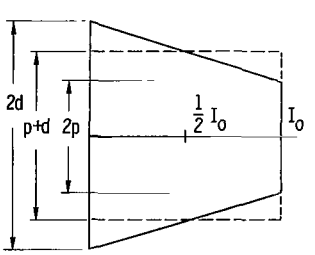

Figure 8. - Beam intensity at detector plane in vertical direction.

From figure 7 and equations II-17 to II-19 of reference 1 the effective height for atoms h_{d_a} is

$$h_{d_a} = (p + d) = h\left(1 + \frac{\ell_c}{\ell_{sd} - \ell_c}\right) \quad \text{(B1)}$$

and the effective height for "holes," h_{d_o} is

$$h_{d_o} = (p + d) = h\left(1 + \frac{\ell_c}{\ell_{sc} + \ell_{sd} - \ell_c}\right) \quad \text{(B2)}$$

Figure 9 shows the horizontal collimation system. From geometry, the effective

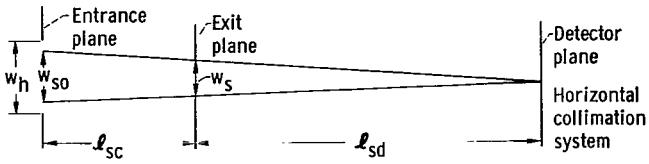

Figure 9. - Horizontal collimation system.

emitting source width for "holes" w_{so} is given by

$$w_{so} = w_s\left(\frac{\ell_{sd} + \ell_{sc}}{\ell_{sd}}\right) \tag{B3}$$

The heights of the emitting atom and "hole" slits h_a and h_h are

$$h_h = h_a = h \tag{B4}$$

Therefore, combining equations (B1) to (B4), with equation (2) yields the following:

The detected atom current

$$I_a = \frac{n\bar{v}e}{4\pi} w_s h_a \frac{1}{(\ell_{sd})^2} w_d h_{d_a} \tag{B5}$$

The detected "hole" current at low densities

$$I_{h_o} = \frac{-n\bar{v}e}{4\pi} w_{so} h_h \frac{1}{(\ell_{sd} + \ell_{sc})^2} w_d h_{d_o} \tag{B6}$$

Replacing w_{so} in (B6) by its value from (B3) and also multiplying (B6) by $\left(h_{d_a}/h_{d_a}\right)$ and (ℓ_{sd}/ℓ_{sd}) allow (B6) to be written as

$$I_{h_o} = -I_a\left(\frac{\ell_{sd}}{\ell_{sd} + \ell_{sc}}\right)\left(\frac{h_{d_o}}{h_{d_a}}\right) \tag{B7}$$

Therefore using equations (3) and (4b), equation (6) of the text is obtained:

$$\frac{I}{I_a} = 1 - \left(\frac{\ell_{sd}}{\ell_{sd} + \ell_{sc}}\right)\left(\frac{h_{d_o}}{h_{d_a}}\right) e^{-n\ell_{sc}Q} \tag{6}$$

where

$$\frac{h_{d_o}}{h_{d_a}} = \frac{\left(1 + \frac{\ell_c}{\ell_{sc} + \ell_{sd} - \ell_c}\right)}{\left(1 + \frac{\ell_c}{\ell_{sd} - \ell_c}\right)} \tag{B8}$$

is the ratio of the effective beam heights at the detector plane for perfect vertical alinement.

REFERENCES

1. Ramsey, Norman Foster: Molecular Beams. Clarendon Press (Oxford), 1956.

2. Taylor, John Bradshaw; and Langmuir, Irving: Vapor Pressure of Cesium by the Positive Ion Method. Phys. Rev., ser. 2, vol. 51, no. 9, May 1, 1937, pp. 753-760.

3. Datz, Sheldon; and Taylor, Ellison H.: Ionization on Platinum and Tungsten Surfaces. I. The Alkali Metals. J. Chem. Phys., vol. 25, no. 3, Sept. 1956, pp. 389-394.

4. Rosin, Seymour; and Rabi, I. I.: Effective Collision Cross Sections of the Alkali Atoms in Various Gases. Phys. Rev., ser. 2, vol. 48, no. 4, Aug. 15, 1935, pp. 373-379.

5. Manista, Eugene J.; and Sheldon, John W.: Preliminary Experiments with a Velocity-Selected Atomic-Beam Apparatus. NASA TN D-2557, 1964.

6. Kusch, P.: Notes on Resolution in Scattering Measurements. J. Chem. Phys., vol. 40, no. 1, Jan. 1, 1964, pp. 1-4.

7. Estermann, I.; Foner, S. N.; and Stern, O.: The Mean Free Paths of Cesium Atoms in Helium, Nitrogen, and Cesium Vapor. Phys. Rev., vol. 71, no. 4, Feb. 1947, pp. 250-257.

3/1 8 / 85

"The aeronautical and space activities of the United States shall be conducted so as to contribute . . . to the expansion of human knowledge of phenomena in the atmosphere and space. The Administration shall provide for the widest practicable and appropriate dissemination of information concerning its activities and the results thereof."

—NATIONAL AERONAUTICS AND SPACE ACT OF 1958

NASA SCIENTIFIC AND TECHNICAL PUBLICATIONS

TECHNICAL REPORTS: Scientific and technical information considered important, complete, and a lasting contribution to existing knowledge.

TECHNICAL NOTES: Information less broad in scope but nevertheless of importance as a contribution to existing knowledge.

TECHNICAL MEMORANDUMS: Information receiving limited distribution because of preliminary data, security classification, or other reasons.

CONTRACTOR REPORTS: Technical information generated in connection with a NASA contract or grant and released under NASA auspices.

TECHNICAL TRANSLATIONS: Information published in a foreign language considered to merit NASA distribution in English.

TECHNICAL REPRINTS: Information derived from NASA activities and initially published in the form of journal articles.

SPECIAL PUBLICATIONS: Information derived from or of value to NASA activities but not necessarily reporting the results of individual NASA-programmed scientific efforts. Publications include conference proceedings, monographs, data compilations, handbooks, sourcebooks, and special bibliographies.

Details on the availability of these publications may be obtained from:

SCIENTIFIC AND TECHNICAL INFORMATION DIVISION

NATIONAL AERONAUTICS AND SPACE ADMINISTRATION

Washington, D.C. 20546